

Onset of chaos in a superconducting Wheatstone bridge of overdamped Josephson junctions

M. Cahay and R. Kothari

Department of Electrical and Computer Engineering, University of Cincinnati, Cincinnati, Ohio 45221-0030

(Received 23 December 1996; revised manuscript received 21 March 1997)

We identify a physical mechanism responsible for the onset of chaos in an asymmetric superconducting Wheatstone bridge of overdamped Josephson junctions while focusing on the dynamics of the transverse junction. The dynamics of the transverse junction are shown to be affected by an effective-noise-current term whose presence eventually leads to the onset of chaos in the bridge. This effective-noise-current term results from the competition of circulating currents in the upper and lower loops of the bridge. For some bridges, the effective-noise-current term has a profound influence on the value of the dc biasing current at which a nonzero average voltage appears across the transverse junction of the bridge. [S0163-1829(97)04430-5]

I. INTRODUCTION

For the last 10 years, Josephson junction arrays have been a benchmark for both the experimental and theoretical study of nonlinear dynamical systems with many degrees of freedom. Since the early 1990s, there has been a growing interest in two-dimensional (2D) arrays following early theoretical predictions of a tremendous increase in the output power of 2D arrays compared to their 1D counterparts.¹ However, up to now, the maximum experimental radiation power of 2D arrays has been found to be much smaller than that of 1D arrays (100 nW maximum versus 50 μ W in 1D arrays).^{2,3} Recently, Wiesenfeld and co-workers formulated general design criteria for optimization of power and linewidth of phase-locked 2D arrays.¹ However, a thorough understanding of phase locking and the effects of disorder on the coherence properties of 2D arrays is still in its infancy. To understand the effects of disorder on synchronization (phase locking) in 2D Josephson junction arrays, there have been recent theoretical investigations of the dynamics of smaller arrays of Josephson junctions (JJ).⁴⁻⁶ For instance, Landsberg *et al.*⁵ have studied two prototype systems—the plaquette and double plaquette of Josephson junctions—and show that, in the presence of moderate disorder in both the critical currents and normal resistances, the vertical junctions within each row can maintain 1:1 frequency locking. On the other hand, different rows operate at different frequencies no matter how small the amount of disorder.

The analysis of JJ arrays still lacks the formulation of general criteria to study the onset of chaos in these arrays in the presence of disorder. This is an important issue since chaos is bound to disrupt phase locking in large arrays. The conditions for the onset of chaos in single underdamped JJ in the presence of radio-frequency current source has been analyzed by Kautz and Monaco.⁷ Extensive numerical simulations by Dominguez and Cerdeira⁸ have pointed out the onset of spatiotemporal chaos in JJ series arrays. However, more general criteria are needed to understand the onset of chaos in 2D and 3D JJ arrays. Towards that end, we present in this paper an extension of our earlier investigations^{9,10} of the dynamics of an array of five junctions forming a superconducting Wheatstone bridge with strong asymmetry (i.e., with dissimilar junction parameters). We show explicitly that the

dynamics of the bridge is characterized by a system of three first-order differential equations, the minimum required for any dynamical system to eventually show signs of chaotic behavior. The origin of chaos in the bridge is clearly identified and linked to the presence of an effective noise current source in the equation governing the dynamics of the transverse junction. We believe our analysis constitutes a preliminary step towards the design of more general criteria to study the onset of chaos in larger JJ arrays.

II. APPROACH

Figure 1 shows a Wheatstone bridge configuration where each cross represents an overdamped Josephson junction. In the limit of negligible capacitance, the dynamic behavior of each junction can be described by the resistively shunted junction model.¹¹ The total current through the *i*th branch, I_i , can be expressed as

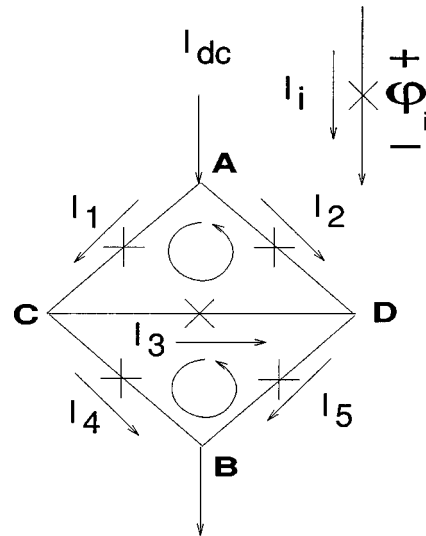


FIG. 1. Wheatstone bridge configuration. Each cross represents a Josephson junction. I_3 is the difference of the two circulating currents in the upper and lower loops of the bridge. Also shown is the convention used to define the polarity of the superconducting phase difference across each Josephson junction.

$$I_i = I_{c;i} \sin \varphi_i + \frac{\hbar}{2eR_i} \left(\frac{d\varphi_i}{dt} \right), \quad (1)$$

where φ_i is the superconducting phase difference across the Josephson junction in the i th branch of the bridge. The quantities $I_{c;i}$ and R_i are the critical current and channel resistance of the i th junction, respectively. The instantaneous voltage across the i th junction is equal to $(\hbar/2e)(d\varphi_i/dt)$. The superconducting Wheatstone bridge is fed by a dc current source (I_{dc}) between nodes A and B in Fig. 1 and the transverse voltage V_{CD} is measured between nodes C and D . For simplicity, we neglect the effects of thermal noise in the junctions.

Using the quantities R_g and I_m to normalize the various resistances and currents inside the bridge¹² and introducing the dimensionless time variable $\tau = \Omega t$ [with $\Omega = (2e/\hbar)R_g I_m$], the total current through the i th branch of the bridge can be rewritten

$$\frac{I_i}{I_m} = \frac{R_g}{R_i} \frac{d\varphi_i}{d\tau} + \frac{I_{c,i}}{I_m} \sin \varphi_i. \quad (2)$$

Using Kirchoff's current law in Fig. 1, we obtain $I_{dc} = I_4 + I_5$, $I_1 = I_3 + I_4$, $I_5 = I_2 + I_3$. If we neglect the self-inductance of each branch and the mutual inductance of the top and bottom loops of the bridge, Kirchoff's voltage law gives

$$U_2 = U_1 + U_3, \quad (3)$$

$$U_4 = U_3 + U_5, \quad (4)$$

where the potential across the i th junction is given by $U_i = R_g I_m (d\varphi_i/d\tau)$. Using Eqs. (2)–(4) and Kirchoff's current law, the dynamics of the bridge can be readily described as a set of five first-order nonlinear differential equations for the φ_i 's. This system of differential equations can be simplified since the φ_i 's are not independent but related by the flux quantization rules written for the upper and lower loops of the Wheatstone bridge. Neglecting the self-inductance of each loop and the mutual inductance between the loops and assuming zero external magnetic field, the flux quantization rule¹¹ applied to the upper and lower loops of the bridge leads to the following constraints:

$$\varphi_1 + \varphi_3 - \varphi_2 = 2\pi n, \quad (5)$$

and

$$\varphi_4 - \varphi_5 - \varphi_3 = 2\pi m, \quad (6)$$

respectively. In Eqs. (5) and (6), n and m are integers. Using Eqs. (5) and (6), the system of first-order nonlinear differential equations for the φ_i 's can then be reduced to a system of three first-order nonlinear differential equations for the variables $x = \varphi_1 + \varphi_2$, $y = \varphi_4 + \varphi_5$, and $z = \varphi_3$. The system of differential equations for the three variables (x, y, z) is derived explicitly in Appendix A:

$$\begin{bmatrix} dx/d\tau \\ dy/d\tau \\ dz/d\tau \end{bmatrix} = \frac{1}{D} \begin{bmatrix} \alpha\delta - \beta^2 & \beta\beta'/2 & \alpha\beta' \\ \beta\beta'/2 & \alpha'\delta - \beta'^2 & \alpha'\beta \\ \beta'\alpha/2 & \beta\alpha'/2 & \alpha\alpha' \end{bmatrix} \begin{bmatrix} b_1 \\ b_2 \\ b_3 \end{bmatrix}. \quad (7)$$

In Eq. (7) above, the following notations were used:¹³

$$b_1 = \frac{I_{dc}}{I_m} - \frac{I_{c;1}}{I_m} \sin\left(\frac{x-z}{2}\right) - \frac{I_{c;2}}{I_m} \sin\left(\frac{x+z}{2}\right), \quad (8)$$

$$b_2 = \frac{I_{dc}}{I_m} - \frac{I_{c;4}}{I_m} \sin\left(\frac{y+z}{2}\right) - \frac{I_{c;5}}{I_m} \sin\left(\frac{y-z}{2}\right), \quad (9)$$

$$b_3 = \frac{1}{2} \frac{I_{c;1}}{I_m} \sin\left(\frac{x-z}{2}\right) - \frac{1}{2} \frac{I_{c;2}}{I_m} \sin\left(\frac{x+z}{2}\right) - \frac{1}{2} \frac{I_{c;4}}{I_m} \sin\left(\frac{y+z}{2}\right) + \frac{1}{2} \frac{I_{c;5}}{I_m} \sin\left(\frac{y-z}{2}\right) - \frac{I_{c;3}}{I_m} \sin z. \quad (10)$$

Furthermore, the following quantities were introduced:

$$D = R_g \left(\frac{\alpha\alpha'}{R_3} + \frac{\alpha\alpha'}{2} (\alpha + \alpha') - \frac{1}{2} (\alpha'\beta^2 + \alpha\beta'^2) \right), \quad (11)$$

$$\alpha = \frac{1}{2} \left(\frac{1}{R_4} + \frac{1}{R_5} \right), \quad \alpha' = \frac{1}{2} \left(\frac{1}{R_1} + \frac{1}{R_2} \right), \quad (12)$$

$$\beta = \frac{1}{2} \left(\frac{1}{R_5} - \frac{1}{R_4} \right), \quad \beta' = \frac{1}{2} \left(\frac{1}{R_1} - \frac{1}{R_2} \right) \quad (13)$$

and

$$\delta = 1/R_3 + (\alpha + \alpha')/2. \quad (14)$$

The quantities α and α' are the average conductances of the two upper and lower JJ 's, respectively. The quantities β and β' characterize the asymmetry in the conductances of the branches of the upper and lower loops of the bridge.

Starting with Eqs. (7)–(14) and using standard units, it can be shown that the phase z satisfies the following equation:

$$\frac{\hbar}{2eR_t} \frac{dz}{dt} + I^* \sin z = I_{dc} + I_N^{\text{eff}}, \quad (15)$$

which is equivalent to the equation of a single junction with a maximum critical supercurrent I^* ,

$$I^* = \frac{2I_{c;3}}{[(R_2 - R_1)/(R_2 + R_1)] + [(R_4 - R_5)/(R_4 + R_5)]}, \quad (16)$$

and with a normal-state resistance

$$R_t = \frac{\beta'\alpha + \alpha'\beta}{2\gamma}, \quad (17)$$

where $\gamma = D/R_g$. In Eq. (15), the effective noise current source I_N^{eff} is given by

$$I_N^{\text{eff}} = \frac{R_4 + R_5}{R_2 R_4 - R_1 R_5} \left[R_1 I_{c;1} \sin\left(\frac{x-z}{2}\right) - R_2 I_{c;2} \sin\left(\frac{x+z}{2}\right) \right] + \frac{R_1 + R_2}{R_2 R_4 - R_1 R_5} \left[R_5 I_{c;5} \sin\left(\frac{y-z}{2}\right) - R_4 I_{c;4} \sin\left(\frac{y+z}{2}\right) \right]. \quad (18)$$

The resistance R_t is the value of the transverse resistance, $R_t = V_{CD}/I_{dc}$, of the Wheatstone bridge fed with a constant current source I_{dc} when only the normal channels of each junction are taken into account as shown in Appendix B.¹⁴

Equation (16) indicates that the supercurrent I^* can be made arbitrarily large by tuning the values of the resistors R_1 , R_2 , R_4 , and R_5 . In fact, according to Eq. (16), I^* is infinite whenever the condition $R_1/R_2 = R_4/R_5$ is satisfied. The latter is the condition for a perfectly balanced bridge when the superconducting channel of each junction is neglected. In that case, the transverse resistance R_t and transverse voltage are both equal to zero.

In Eq. (15), the effective noise current source I_N^{eff} is given by

$$I_N^{\text{eff}} = \frac{R_4 + R_5}{R_2 R_4 - R_1 R_5} \left[R_1 I_{c;1} \sin\left(\frac{x-z}{2}\right) - R_2 I_{c;2} \sin\left(\frac{x+z}{2}\right) \right] + \frac{R_1 + R_2}{R_2 R_4 - R_1 R_5} \left[R_5 I_{c;5} \sin\left(\frac{y-z}{2}\right) - R_4 I_{c;4} \sin\left(\frac{y+z}{2}\right) \right]. \quad (19)$$

It is instructive to rewrite the effective noise current source as

$$I_N^{\text{eff}} = \frac{2}{\beta'/\alpha' + \beta/\alpha} [(R_1 I_{c;1} \sin\varphi_1 - R_2 I_{c;2} \sin\varphi_2) - (R_4 I_{c;4} \sin\varphi_4 - R_5 I_{c;5} \sin\varphi_5)], \quad (20)$$

which shows that I_N^{eff} is due to the asymmetry in the bridge parameters leading to a competition of two circulating supercurrents in the top and bottom loops of the bridge.

III. RESULTS

Three numerical examples of the current-transverse voltage characteristics ($I_{dc} - V_{CD}$) of various Wheatstone bridges are shown as full lines in Fig. 2. The parameters of the first bridge W_I are listed in Table I.¹⁵ In this bridge, the transverse junction has the same parameters as the junction with the largest critical supercurrent in the other branches. The other two bridges are identical to W_I except for the transverse junction. In bridge W_{II} the transverse junction has the same parameters as junction 1 (with the intermediate critical supercurrent) and, in bridge W_{III} , the transverse junction has the same parameters as junction 4 (with the lowest critical supercurrent).

As shown in Fig. 2, for some bridges, the $I_{dc} - V_{CD}$ characteristics at $T=0$ K can be well approximated by the current-voltage characteristics of a single junction characterized by the parameters (I^* , R_t). These $I-V$ curves are calculated using Eq. (15) while neglecting the terms I_N^{eff} and are shown as dash-dotted lines in Fig. 2. For the bridges W_{II} and

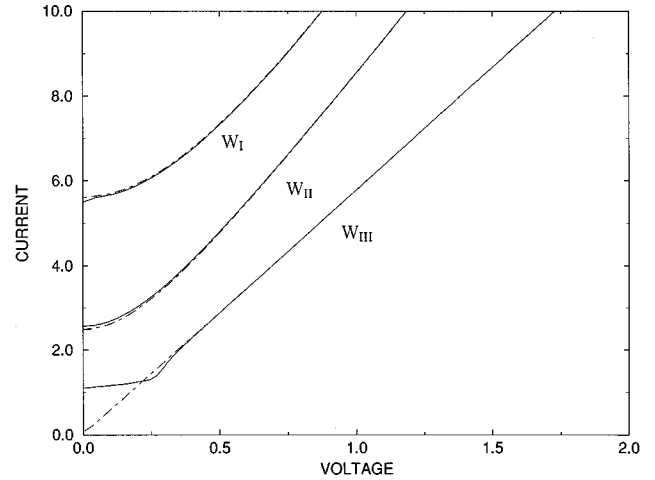


FIG. 2. The full lines are the current-transverse voltage characteristics of the three Wheatstone bridges with the parameters listed in Table I. The dash-dotted lines are the current-voltage characteristics of a single junction with the parameters (R_t, I^*) while neglecting the effective noise current source in Eq. (15). Currents and voltages are expressed in units of $I_{c;2}$ and $V_0 = R_2 I_{c;2}$.

W_{III} the effective noise current source becomes increasingly important. This is expected from Eqs. (16) and (18) since, when $I_{c;3}$ is smaller than all other $I_{c;i}$'s, I_N^{eff} is not negligible in Eq. (15). This trend is not particular to the specific bridges studied here and holds true for other bridges whose middle junction has the smallest critical supercurrent. Numerically, the values of the maximum critical supercurrent in the $I_{dc} - V_{CD}$ characteristics are found to be equal to $159.6 \mu\text{A}$ ($5.7I_{c;2}$) for bridge W_I , $72.2 \mu\text{A}$ ($2.58I_{c;2}$) for bridge W_{II} , and $30.2 \mu\text{A}$ ($1.08 I_{c;2}$) for bridge W_{III} , where $I_{c;2}$ is the maximum critical supercurrent. Equation (16), on the other hand, gives a critical supercurrent I^* equal to $156.4 \mu\text{A}$ ($5.6I_{c;2}$) for bridge W_I , $69.8 \mu\text{A}$ ($2.49I_{c;2}$) for bridge W_{II} , and $2.6 \mu\text{A}$ ($0.09I_{c;2}$) for bridge W_{III} .

I_N^{eff} is a highly nonlinear function of the three variables (x, y, z) which is bounded and independent of I_{dc} , at least explicitly. It is a function of the normal-state resistances and critical supercurrents in all branches other than the transverse one. Since there are two positive and two negative terms in the expression of I_N^{eff} , we expect it to swing in the positive and negative directions as a function of time. The change in sign of I_N^{eff} is dependent on the time scales controlling the

TABLE I. The supercurrent and normal resistance values of the Wheatstone bridge W_I . The second bridge (W_{II}) has the same junction parameters as the first one except for the transverse junction whose parameters are the same as for junction 1. For the third bridge (W_{III}), the junction parameters are the same as for junction 4.

Junction	$I_{c;i}$ (μA)	R_i (Ω)
1	12.5	12.5
2	28.0	9.6
3	28.0	9.6
4	0.47	28.0
5	28.0	9.6

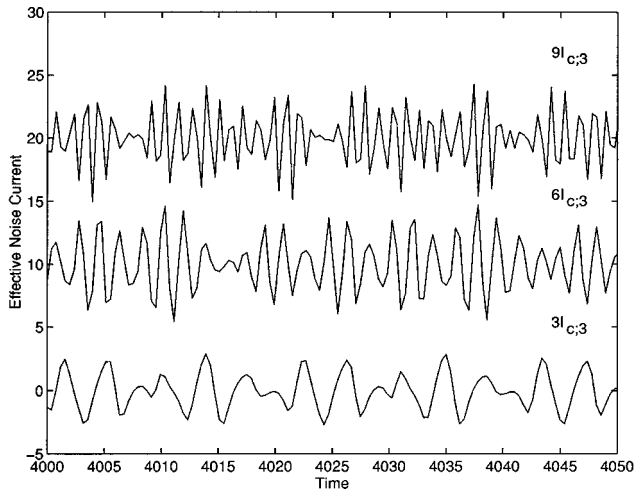


FIG. 3. Time dependence of the effective noise current source I_N^{eff} as a function of the dc biasing current of the Wheatstone bridge W_I . For clarity, the curves corresponding to $I_{\text{dc}} = 6$ and $9 I_{c;3}$ have been shifted vertically by an amount equal to 10 and $20 I_{c;3}$, respectively. Time is expressed in units of $\hbar/2eR_3 I_{c;3}$.

dynamics of the Wheatstone bridge. Figure 3 shows a plot of I_N^{eff} versus time for different values of the dc biasing current of the bridge W_I . Figure 3 shows that the effective noise current source I_N^{eff} has a maximum amplitude merely independent of the dc biasing current and its variation occurs over a smaller time scale as I_{dc} increases. This is due to nearly linear increase with time of both variables x and y , solutions of the system of differential equations (7). The linear increase with time of x and y for large values of I_{dc} follows directly from Eq. (7) if the terms proportional to the critical supercurrents in the expressions of the b_i 's are neglected. The nearly linear increase with time of x and y was confirmed numerically for all the bridges simulated here. Typical results are shown in Fig. 4 for Wheatstone bridge W_I at two different values of I_{dc} . Referring to Eq. (18), since x and y are found to be proportional to I_{dc} , this explains the higher frequency components in the plot of I_N^{eff} versus time in Fig. 3 for larger I_{dc} .

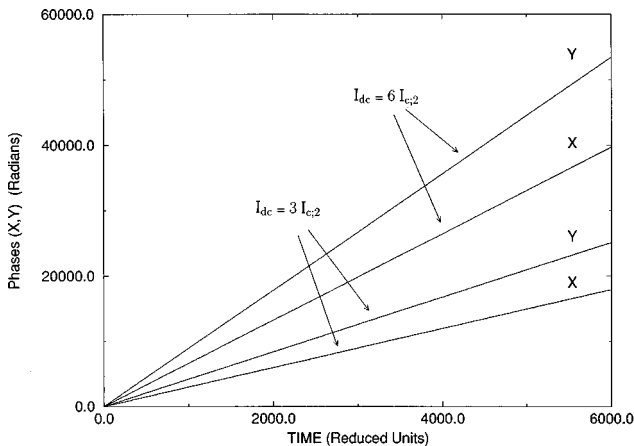


FIG. 4. Time dependence of the variable x and y solutions of the system of differential equations (7) for two different values of the dc biasing current. The bridge simulated is bridge W_I . At large I_{dc} , both x and y increase linearly with time. Time is expressed in units of $\hbar/2eR_3 I_{c;3}$.

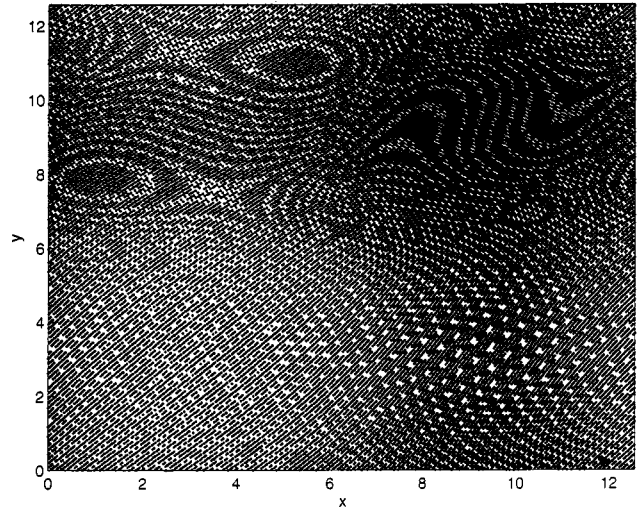


FIG. 5. Two-sided Poincaré map showing the values of the variables $(x,y) \bmod(4\pi)$ for each crossing of the plane $z = 2\pi$ by the trajectory describing the dynamics of the Wheatstone bridge W_{III} . The dc biasing current is set equal to $6 I_{c;2}$.

Since the dynamics of the bridge can be reduced to a set of three highly nonlinear differential equations, there exists a possibility to observe the onset of chaos in the bridge while varying the dc biasing current. The onset of chaos can be illustrated through the computation of Poincaré maps for the system of differential equations for the variables (x,y,z) as a function of I_{dc} . Using Eqs. (8)–(10), it can be seen that the system of differential equations (7) is invariant under the change of variables $(x,y,z) \rightarrow (x+4\pi, y+4\pi, z+4\pi)$. We computed a two-sided Poincaré map by recording the values of the phases $(x,y) \bmod(4\pi)$ at time τ corresponding to crossings of the plane $z = 2\pi$ (in either direction) by the trajectory initiating at $(0,0,0)$. This two-sided Poincaré map is shown in Fig. 5 for I_{dc} equal to $6 I_{c;2}$ for bridge W_{III} . This Poincaré map clearly indicates the presence of chaos in the bridge. Indeed, while plotting Fig. 5 for a chaotic solution, the successive values of the phases $(x,y) \bmod(4\pi)$ recorded as described above were found to jump from one region to another of the interval $[0,4\pi] \times [0,4\pi]$ in an apparently random fashion, producing a geometrically complex Poincaré section, often referred to as a strange attractor. The onset of chaos in the bridge was supported through a calculation of the one-dimensional Lyapounov exponents which characterize the divergence (positive exponent) or convergence (negative exponent) of neighboring trajectory solutions of the system of differential equations for the variables (x,y,z) .^{16,17} The Lyapounov exponents were computed using the algorithm developed by Wolf *et al.*¹⁶ A brief description of the algorithm used to calculate the Lyapounov exponents is given in Appendix C.

Figure 6(a) is a plot of the three Lyapounov exponents of the system of differential equations (7) as a function of I_{dc} for bridge W_I . Figure 6(b) is a look at the Lyapounov exponents in a narrower window showing that one Lyapounov exponent becomes positive when I_{dc} increases above $I_{c;4} + I_{c;5}$. This threshold corresponds to a value of I_{dc} larger than the maximum supercurrent which can flow through the superconducting Wheatstone bridges considered here. Past $I_{c;4} + I_{c;5}$, one Lyapounov exponent stays positive for the

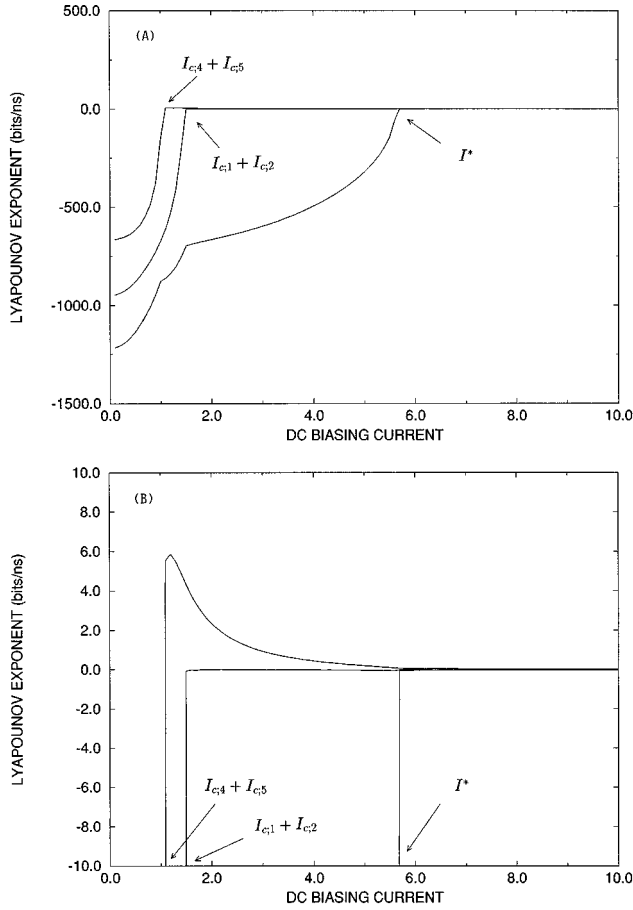


FIG. 6. (a) Plot of the three Lyapounov exponents of the system of differential equations (7) as a function of I_{dc} for bridge W_I . (b) Zoom on the variation of the Lyapounov exponents within a smaller range of values showing that one Lyapounov exponent becomes positive when I_{dc} increases above $I_{c;4} + I_{c;5}$. This is the threshold corresponding to a dc biasing current larger than the maximum supercurrent which can flow through the superconducting Wheatstone bridge.

range of I_{dc} investigated here. For all bridges, the Lyapounov exponents were found to be quite small above the critical supercurrent I^* at which a nonzero value of the average transverse voltage (V_{CD}) appears across the bridge. Numerically, the sum of the three Lyapounov exponents was found to be negative for all I_{dc} 's, as required for any dissipative system.¹⁸

IV. CONCLUSIONS

In conclusion, we have identified a physical mechanism leading to the onset of chaos in an asymmetric superconducting Wheatstone bridge of overdamped Josephson junctions as the presence of an effective noise current source in the equation describing the dynamics of the transverse junction of the bridge. This effective noise current source results from the competition of circulating supercurrents in the upper and lower loops of the bridge. The onset of chaos in the bridge is found to occur at the dc biasing current corresponding to the maximum supercurrent which can flow through the bridge. We believe that the analysis performed here could be extended to larger arrays of Josephson junctions

providing additional insight on the mechanisms disrupting the intralocking of JJ's in 2D or 3D arrays in the presence of disorder.

APPENDIX A

In this appendix, we outline the derivation of the system of differential equations (7) in the text. Applying Kirchoff's current law to the nodes of the bridge in Fig. 1, we obtain

$$I = I_1 + I_2, \quad (A1)$$

$$I_1 = I_3 + I_4, \quad (A2)$$

$$I_5 = I_2 + I_3, \quad (A3)$$

and

$$I = I_4 + I_5. \quad (A4)$$

Furthermore, introducing the quantities: $\Omega = (2e/\hbar)R_g I_m$ and $\tau = \Omega t$, the voltage across the i th junction can be written

$$U_i = R_g I_m \frac{d\varphi_i}{d\tau}, \quad (A5)$$

and the current through the i th branch is given by

$$\frac{I_i}{I_m} = \frac{R_i}{R_g} \frac{d\varphi_i}{d\tau} + \frac{I_{c;i}}{I_m} \sin\varphi_i. \quad (A6)$$

Equations (A2) and (A3) can then be written as follows:

$$\begin{aligned} \frac{R_1}{R_g} \frac{d\varphi_1}{d\tau} + \frac{I_{c;1}}{I_m} \sin\varphi_1 \\ = \frac{R_3}{R_g} \frac{d\varphi_3}{d\tau} + \frac{I_{c;3}}{I_m} \sin\varphi_3 + \frac{R_4}{R_g} \frac{d\varphi_4}{d\tau} + \frac{I_{c;4}}{I_m} \sin\varphi_4, \end{aligned} \quad (A7)$$

$$\begin{aligned} \frac{R_5}{R_g} \frac{d\varphi_5}{d\tau} + \frac{I_{c;5}}{I_m} \sin\varphi_5 \\ = \frac{R_2}{R_g} \frac{d\varphi_2}{d\tau} + \frac{I_{c;2}}{I_m} \sin\varphi_2 + \frac{R_3}{R_g} \frac{d\varphi_3}{d\tau} + \frac{I_{c;3}}{I_m} \sin\varphi_3. \end{aligned} \quad (A8)$$

Summing the last two equations and rearranging, we obtain

$$\begin{aligned} 2 \left(\frac{R_3}{R_g} \frac{d\varphi_3}{d\tau} + \frac{I_{c;3}}{I_m} \sin\varphi_3 \right) \\ = \frac{R_5}{R_g} \frac{d\varphi_5}{d\tau} - \frac{R_4}{R_g} \frac{d\varphi_4}{d\tau} + \frac{R_1}{R_g} \frac{d\varphi_1}{d\tau} - \frac{R_2}{R_g} \frac{d\varphi_2}{d\tau} + \frac{I_{c;1}}{I_m} \sin\varphi_1 \\ - \frac{I_{c;2}}{I_m} \sin\varphi_2 + \frac{I_{c;5}}{I_m} \sin\varphi_5 - \frac{I_{c;4}}{I_m} \sin\varphi_4. \end{aligned} \quad (A9)$$

Making use of the two constraints (5) and (6) in the text and the definitions (12) and (13), Eq. (A9) can be rewritten as follows:

$$R_g \left[\frac{1}{R_3} + \left(\frac{\alpha + \alpha'}{2} \right) \right] \frac{d\varphi_3}{d\tau} + \frac{I_{c;3}}{I_m} \sin\varphi_3 = \frac{R_g}{2} \left[\beta' \left(\frac{d\varphi_5}{d\tau} + \frac{d\varphi_4}{d\tau} \right) + \beta \left(\frac{d\varphi_1}{d\tau} + \frac{d\varphi_2}{d\tau} \right) \right] + \frac{1}{2} \left[\frac{I_{c;1}}{I_m} \sin \left(\frac{\varphi_1 + \varphi_2 - \varphi_3}{2} \right) - \frac{I_{c;2}}{I_m} \sin \left(\frac{\varphi_1 + \varphi_2 + \varphi_3}{2} \right) \right] + \frac{1}{2} \left[\frac{I_{c;5}}{I_m} \sin \left(\frac{\varphi_4 + \varphi_5 - \varphi_3}{2} \right) - \frac{I_{c;4}}{I_m} \sin \left(\frac{\varphi_4 + \varphi_5 + \varphi_3}{2} \right) \right]. \quad (\text{A10})$$

Defining $z = \varphi_3$, $x = \varphi_1 + \varphi_2$, and $y = \varphi_4 + \varphi_5$, the last equation becomes

$$R_g \left[\frac{1}{R_3} + \left(\frac{\alpha + \alpha'}{2} \right) \right] \frac{dz}{d\tau} + \frac{I_{c;3}}{I_m} \sin z = \frac{R_g}{2} \left(\beta' \frac{dy}{d\tau} + \beta \frac{dx}{d\tau} \right) + \frac{1}{2} \left[\frac{I_{c;1}}{I_m} \sin \left(\frac{x-z}{2} \right) - \frac{I_{c;2}}{I_m} \sin \left(\frac{x+z}{2} \right) \right] + \frac{1}{2} \left[\frac{I_{c;5}}{I_m} \sin \left(\frac{y-z}{2} \right) - \frac{I_{c;4}}{I_m} \sin \left(\frac{y+z}{2} \right) \right]. \quad (\text{A11})$$

The differential equations for the dynamical variables x and y are derived easily starting from Eqs. (A1) and (A4). Solving these equations simultaneously with Eq. (A11), the expressions $dx/d\tau, dy/d\tau, dz/d\tau$ are then readily found to be given by Eq. (7) in text.

APPENDIX B

For an unbalanced (nonsuperconducting) Wheatstone bridge, the transverse resistance, $R_t = V_{CD}/I_{dc}$, can be readily calculated using the $\Delta - Y$ connection rules.¹⁴ As shown in Fig. 7, this technique consists in replacing the Δ network of resistors (R_1, R_2, R_3) by an equivalent Y network of resistors (R'_1, R'_2, R'_3) whose values are given explicitly by¹⁴

$$R'_1 = \frac{R_2 R_3}{R_1 + R_2 + R_3}, \quad (\text{B1})$$

$$R'_2 = \frac{R_1 R_3}{R_1 + R_2 + R_3}, \quad (\text{B2})$$

and

$$R'_3 = \frac{R_1 R_2}{R_1 + R_2 + R_3}. \quad (\text{B3})$$

Application of network analysis to the equivalent circuit in Fig. 6 leads to the following result for the transverse resistance:

$$R_t = \frac{V_{CD}}{I_{dc}} = \frac{R_3(R_2 R_4 - R_1 R_5)}{(R_4 + R_5)(R_1 + R_2 + R_3) + R_3(R_1 + R_2)}. \quad (\text{B4})$$

The latter can be written in the more compact form given by Eq. (17) by using definitions (12) and (13).

APPENDIX C

For an n th-order system, we must solve

$$\dot{x} = f(x, t), \quad x(t_0) = x_0, \quad (\text{C1})$$

where x has n dimensions. If we call $\phi_t(x_0, t_0)$, the solution of this system of differential equations for the specified ini-

tial condition $x(t_0)$, the determination of the Lyapounov spectrum of a dynamical system requires $D_{x_0} \phi_t(x_0, t_0)$, the derivative of the trajectory with respect to the initial condition. From Eq. (C1), we have

$$\dot{\phi}_t(x_0, t_0) = f[\phi_t(x_0, t_0), t], \quad \phi_{t_0}(x_0, t_0) = x_0. \quad (\text{C2})$$

Differentiating Eq. (C2) with respect to x_0 , we obtain

$$D_{x_0} \dot{\phi}_t(x_0, t_0) = D_x f[\phi_t(x_0, t_0), t] D_{x_0} \phi_t(x_0, t_0),$$

$$D_{x_0} \phi_{t_0}(x_0, t_0) = I. \quad (\text{C3})$$

Introducing $\Phi_t(x_0, t_0) = D_{x_0} \phi_t(x_0, t_0)$, Eq. (C3) becomes

$$\dot{\Phi}_t(x_0, t_0) = D_x f[\phi_t(x_0, t_0), t] \Phi_t(x_0, t_0), \quad \Phi_{t_0}(x_0, t_0) = I, \quad (\text{C4})$$

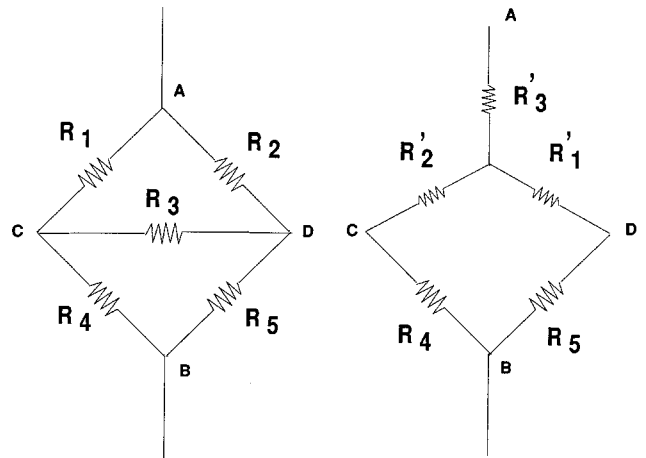


FIG. 7. Illustration of the $\Delta - Y$ connection rule (Ref. 14) to calculate the transverse resistance $R_t = V_{CD}/I_{dc}$. In this technique, the Δ network of resistors (R_1, R_2, R_3) is first replaced by the equivalent Y network of resistors (R'_1, R'_2, R'_3). The transverse resistance R_t is then derived using Kirchoff's current and voltage laws for the equivalent circuit as shown in Appendix B.

which is the variational equation. This variational equation depends both on ϕ and Φ_0 . The system of differential equations and the variational equation must be solved simultaneously. To perform this simultaneous integration, the variational equation is appended to the original system to obtain the combined system

$$\begin{bmatrix} \dot{x} \\ \dot{\Phi} \end{bmatrix} = \begin{bmatrix} f(x,t) \\ D_x f(x,t)\Phi \end{bmatrix}, \quad (\text{C5})$$

which is the integrated subject to the initial conditions

$$\begin{bmatrix} x(t_0) \\ \Phi(t_0) \end{bmatrix} = \begin{bmatrix} x_0 \\ I \end{bmatrix}. \quad (\text{C6})$$

An explicit algorithm to calculate the Lyapounov spectrum for a nonlinear system whose equations of motion and their linearizations [Eq. (C6)] are provided by the user has been given by Wolf and co-workers.¹⁶ The technique is based on the calculation of the long-term growth rate of small volume elements on the attractor. The reader is referred to Appendix A of Ref. 16 for a detailed description of the algorithm. For the case under study, we need the Jacobian $[D_x f(x,t)]$ in Eq. (C6) for the system of differential equations (7) describing the dynamics of the bridge. This Jacobian is calculated explicitly in the next appendix.

APPENDIX D

As shown in Sec. II, the dynamics of the bridge can be described by a set of three first-order differential equations:

$$\dot{x} = F_X(x,y,z), \quad (\text{D1})$$

$$\dot{y} = F_Y(x,y,z), \quad (\text{D2})$$

$$\dot{z} = F_Z(x,y,z), \quad (\text{D3})$$

where the explicit forms of F_X, F_Y, F_Z are given in Eq. (7) in Sec. II. A calculation of the Lyapounov exponents for this system of differential equations requires a numerical solution of the variational equation, as described in Appendix C. This variational equation requires an explicit calculation of the Jacobian associated to the right-hand side of the three differential equations above. The elements of the Jacobian can be calculated explicitly and are found to be

$$\frac{dF_X}{dx} = \left(\alpha\delta - \frac{\beta^2}{2} \right) \frac{db_1}{dx} + \alpha\beta' \frac{db_3}{dx}, \quad (\text{D4})$$

$$\frac{dF_Y}{dy} = \left(\frac{\beta\beta'}{2} \right) \frac{db_2}{dy} + \alpha\beta' \frac{db_3}{dy}, \quad (\text{D5})$$

$$\frac{dF_X}{dz} = \left(\alpha\delta - \frac{\beta^2}{2} \right) \frac{db_1}{dz} + \frac{\beta'\beta}{2} \frac{db_2}{dz} + \alpha\beta' \frac{db_3}{dz}, \quad (\text{D6})$$

$$\frac{dF_Y}{dx} = \frac{\beta\beta'^2}{2} \frac{db_1}{dx} + \alpha'\beta \frac{db_3}{dx}, \quad (\text{D7})$$

$$\frac{dF_Y}{dy} = \left(\alpha'\delta - \frac{\beta'}{2} \right) \frac{db_2}{dy} + \alpha'\beta \frac{db_3}{dy}, \quad (\text{D8})$$

$$\frac{dF_Y}{dz} = \frac{\beta\beta'}{2} \frac{db_1}{dz} + \left(\alpha'\delta - \frac{\beta'^2}{2} \right) \frac{db_2}{dz} + \alpha'\beta \frac{db_3}{dz}, \quad (\text{D9})$$

$$\frac{dF_Z}{dx} = \frac{\alpha\beta'}{2} \frac{db_1}{dx} + \alpha\alpha' \frac{db_3}{dx}, \quad (\text{D10})$$

$$\frac{dF_Z}{dy} = \frac{\alpha'\beta}{2} \frac{db_2}{dy} + \alpha\alpha' \frac{db_3}{dy}, \quad (\text{D11})$$

$$\frac{dF_Z}{dz} = \frac{\alpha\beta'}{2} \frac{db_1}{dz} + \frac{\alpha'\beta}{2} \frac{db_2}{dz} + \alpha\alpha' \frac{db_3}{dz}, \quad (\text{D12})$$

where $\delta = 1/R_{n,3} + [(\alpha + \alpha'/2)]$.

The explicit expressions for (b_1, b_2, b_3) are given by Eqs. (8)–(10) in Sec. II. The derivatives of (b_1, b_2, b_3) appearing in the elements of the Jacobian matrix can be found exactly;

$$\frac{db_1}{dx} = -\frac{Ic_1}{I_m} \cos\left(\frac{x-z}{2}\right) - \frac{Ic_2}{I_m} \cos\left(\frac{x+z}{2}\right), \quad (\text{D13})$$

$$\frac{db_1}{dy} = 0, \quad (\text{D14})$$

$$\frac{db_1}{dz} = \frac{Ic_1}{I_m} \cos\left(\frac{x-z}{2}\right) - \frac{Ic_2}{I_m} \cos\left(\frac{x+z}{2}\right), \quad (\text{D15})$$

$$\frac{db_2}{dx} = 0, \quad (\text{D16})$$

$$\frac{db_2}{dy} = -\frac{Ic_4}{I_m} \cos\left(\frac{y+z}{2}\right) - \frac{Ic_5}{I_m} \cos\left(\frac{y-z}{2}\right), \quad (\text{D17})$$

$$\frac{db_2}{dz} = -\frac{Ic_4}{I_m} \cos\left(\frac{y+z}{2}\right) + \frac{Ic_5}{I_m} \cos\left(\frac{y-z}{2}\right), \quad (\text{D18})$$

$$\frac{db_3}{dx} = \frac{1}{2} \frac{db_1}{dz}, \quad (\text{D19})$$

$$\frac{db_2}{dy} = \frac{1}{2} \frac{db_2}{dz}, \quad (\text{D20})$$

$$\frac{db_3}{dz} = \frac{1}{2} \frac{db_2}{dy} + \frac{1}{2} \frac{db_1}{dx} - \frac{Ic_3}{I_m} \cos z. \quad (\text{D21})$$

- ¹K. Wiesenfeld, S. P. Benz, and P. A. A. Booi, *J. Appl. Phys.* **76**, 3835 (1994).
- ²S. P. Benz and C. J. Burroughs, *Appl. Phys. Lett.* **58**, 2162 (1991).
- ³J. A. Stern, H. G. LeDuc, and J. Zmudzin, *Trans. Appl. Supercond.* **3**, 2485 (1993).
- ⁴B. H. Larsen and S. P. Benz, *Appl. Phys. Lett.* **66**, 3209 (1995).
- ⁵A. S. Landsberg, Y. Braiman, and K. Wiesenfeld, *Appl. Phys. Lett.* **67**, 1935 (1995).
- ⁶M. Basler, W. Krech, and K. Yu. Platov, *Phys. Rev. B* **52**, 7504 (1995).
- ⁷R. L. Kautz and R. Monaco, *J. Appl. Phys.* **57**, 875 (1985).
- ⁸D. Dominguez and H. A. Cerdeira, *Phys. Rev. B* **52**, 513 (1995).
- ⁹G. Qian, M. Cahay, and R. Kothari, *J. Appl. Phys.* **75**, 3217 (1994).
- ¹⁰M. Cahay, G. Qian, and R. Kothari, *J. Appl. Phys.* **78**, 2581 (1995).
- ¹¹T. P. Orlando and K. A. Delin, *Foundations of Applied Superconductivity* (Addison-Wesley, Reading, MA, 1991).
- ¹²In our numerical examples, we choose R_g and I_m equal to R_3 and $I_{c;3}$ of Wheatstone bridge W_1 whose parameters are listed in Table I. These parameters characterize the junction with the largest critical current in the superconducting Wheatstone bridges considered in our numerical examples and are therefore appropriate scaling parameters for all junctions in the bridge.
- ¹³The fixed points of Eq. (7) are determined by setting the right-hand side to zero. Since the determinant of the matrix on the right-hand side is nonzero for the Wheatstone bridges analyzed here, the fixed points must satisfy the following equations:
- $$b_1 = b_2 = b_3 = 0.$$
- The condition $b_1 = 0$ is satisfied if phases φ_1 and φ_2 can be found such that
- $$I_{dc} = I_{c;1} \sin \varphi_1 + I_{c;2} \sin \varphi_2.$$
- Similarly, the condition $b_2 = 0$ is satisfied if phases φ_4 and φ_5

exist such that

$$I_{dc} = I_{c;4} \sin \varphi_4 + I_{c;5} \sin \varphi_5.$$

The last two equations will have real solutions as long as $I_{dc} < \min(I_{c;1} + I_{c;2}, I_{c;4} + I_{c;5})$, i.e., whenever the dc biasing current is kept under the lowest of the two maximum total critical supercurrent allowed to flow in the upper and bottom two junctions. Past that value of I_{dc} , the conditions $b_1 = b_2 = 0$ can no longer be satisfied and the system of differential equations (7) has no more fixed points. The condition $b_3 = 0$ is equivalent to

$$I_{c;3} \sin z = \frac{1}{2}(I_{c;1} \sin \varphi_1 - I_{c;2} \sin \varphi_2) - \frac{1}{2}(I_{c;4} \sin \varphi_4 - I_{c;5} \sin \varphi_5)$$

expressing the supercurrent flowing through the transverse junction of the bridge as the difference of the two circulating supercurrents in the upper and lower loops of the bridge. Past the threshold value of I_{dc} either (φ_1, φ_2) or (φ_4, φ_5) would become time varying and therefore no constant z can satisfy the condition $b_3 = 0$, in agreement with our earlier conclusion that fixed points can no longer exist in that case. Numerical simulations show that the condition $b_3 = 0$ no longer holds when $I_{dc} > \min(I_{c;1} + I_{c;2}, I_{c;4} + I_{c;5})$.

- ¹⁴R. L. Boylestad, *Introductory Circuit Analysis*, 6th ed. (Merrill, Columbus, OH, 1990), p. 266.
- ¹⁵The values of the critical currents and normal-state resistances selected in our numerical simulations are the values calculated for different gate voltages for the T -gate superconducting field effect transistor modeled by H. Lai, G. Qian, and M. Cahay, *J. Appl. Phys.* **73**, 3560 (1993).
- ¹⁶A. Wolf, J. B. Swift, H. L. Swinney, and J. A. Vastano, *Physica D* **16**, 285 (1985).
- ¹⁷I. Shimada and T. Nagashima, *Prog. Theor. Phys.* **61**, 1605 (1979).
- ¹⁸See T. S. Parker and L. O. Chua, *Practical Numerical Algorithms for Chaotic Systems* (Springer-Verlag, New York, 1989), Chap. 3.